JOINT CONFERENCE PROCEEDINGS
7th International Conference on Urban Earthquake Engineering (7CUEE) &
5th International Conference on Earthquake Engineering (5ICEE)
March 3-5, 2010, Tokyo Institute of Technology, Tokyo, Japan

ANALYSIS OF LOVE-WAVE COMPONENTS IN MICROTREMORS

Taku Tada[1], Ikuo Cho[2], and Yuzo Shinozaki[3]

1) Technical Staff Member, Geological Survey of Japan, National Institute of Advanced Industrial Science and Technology (AIST), Japan
2) Research Scientist, Geological Survey of Japan, National Institute of Advanced Industrial Science and Technology (AIST), Japan
3) Professor, Department of Architecture, Faculty of Engineering, Tokyo University of Science, Japan
kogutek@ni.aist.go.jp, ikuo-chou@aist.go.jp, sinozaki@rs.kagu.tus.ac.jp

Abstract: We present new and simple formulas, obtained by expanding the SPAC method, that allow one to infer (1) Love-wave phase velocities and (2) Rayleigh-to-Love power partition ratios using records of microtremors around a circle and at its center. Love-wave velocities can be inferred by simple inversion of an observational equation that involves Bessel functions. Two-component horizontal-motion records are the only input required. Rayleigh-to-Love power partition ratios can be inferred by simple forward algebra. Vertical- and radial-component horizontal-motion records around a circle, plus three-component records at its center, suffice for this purpose. We have released BIDO, a package of free software, that automatically implements the SPAC method plus a broad variety of circular-array microtremor techniques that we have so far developed on its basis. Application of the BIDO software to field data from two sites in Japan indicates preponderance of Love-wave components over Rayleigh-wave components in horizontal-motion microtremors, although further investigations are necessary before any conclusion can be drawn with certainty.

1. INTRODUCTION

The spatial autocorrelation (SPAC) method is a popular technique of microtremor (ambient noise) exploration that employs circular arrays (Aki 1957, Okada 2006, Cho et al. 2008). It is most typically used to infer phase velocities of Rayleigh waves (c^R) using vertical-motion records of microtremors (e.g. Ekström et al. 2009, Picozzi et al. 2009, Prieto et al. 2009, Stephenson et al. 2009; see references in Cho et al. 2008 and Tada et al. 2009 for more).

A derivative form of the technique, known as the three-component SPAC method because it relies on the use of three-component microtremor records, provides the possibility to simultaneously infer (i) c^R, (ii) phase velocities of Love waves (c^L), and (iii) ratios of power partition between Rayleigh waves and Love waves (Okada and Matsushima 1989, Ferrazzini et al. 1991, Endrun et al. 2010). Availability of information related to Love-wave properties, such as (ii) c^L and the (iii) power partition ratios, should provide better constraint on subsurface soil structures than when (i) c^R alone is available. In the three-component SPAC method, however, a nonlinear set of simultaneous equations has to be solved for the three unknown parameters, so that the solution process can be fairly complicated.

By expanding the SPAC method, we have recently developed novel formulas that allow one to infer c^L independently by simple inversion of an observational equation, and also to infer Rayleigh-to-Love power partition ratios independently by simple forward algebra, with no need to solve simultaneous equations (Tada et al. 2009). Just like in the case of the SPAC method, records of microtremors around a circle and at its center are all that is required of the input. Two-component horizontal-motion records suffice for the estimation of c^L, whereas vertical- and one-component horizontal-motion records around the circle, plus three-component records at its center, suffice for the estimation of the power partition ratios. Our new methods therefore substantially facilitate the evaluation of Love-wave properties using circular microtremor arrays.

This article reviews the flow of algorithm in our new techniques, and presents examples of field data analysis results, with relative emphasis on the Rayleigh-to-Love power partition ratios.

2. METHOD DESCRIPTIONS

2.1 Method for Estimating Love-Wave Velocities (the SPAC+L Method)

Let $R(t, r, \theta)$ and $T(t, r, \theta)$ be the radial and tangential components, respectively, of the horizontal-motion seismogram of microtremors at radius r and azimuth θ as seen from the array center. The sign of $R(t, r, \theta)$ is taken to be positive in the centrifugal direction, whereas $T(t, r, \theta)$ is taken to be positive in the counterclockwise direction.

We define $R_1(t, r)$ as a weighted average of $R(t, r, \theta)$ over the azimuth θ:

$$R_1(t,r) = \int_{-\pi}^{\pi} R(t,r,\theta)\exp(-i\theta)d\theta\,. \qquad (1)$$

In the special case of $r = 0$, Eq. (1) reduces to

$$R_1(t,0) = \pi[R(t,0,0) - iT(t,0,0)] \quad (2)$$

(Tada et al. 2009, eq. 8). We also define $T_0(t, r)$ as a non-weighted azimuthal average of $T(t, r, \theta)$:

$$T_0(t,r) = \int_{-\pi}^{\pi} T(t,r,\theta)d\theta . \quad (3)$$

Our formula for evaluating Love-wave phase velocities $c^L(\omega)$, which vary with frequency ω, is

$$\frac{G_{R1T0}(r,r;\omega)}{G_{R1T0}(0,r;\omega)} = J_0(r\omega / c^L(\omega)) + J_2(r\omega / c^L(\omega)), \quad (4)$$

where $G_{R1T0}(r, r; \omega)$ is the cross-spectral density between $R_1(t, r)$ and $T_0(t, r)$; $G_{R1T0}(0, r; \omega)$ is the cross-spectral density between $R_1(t, 0)$ and $T_0(t, r)$; and $J_m(\cdot)$ denotes the mth-order Bessel function of the first kind. Eq. (4) holds true under the assumption that the field of Love waves is dominated by a single mode (most typically the fundamental mode, but not necessarily). The c^L evaluation method, based on the use of Eq. (4), was named by Tada et al. (2009) the "SPAC+L method," where the plus sign refers to the one that appears on the right-hand side of Eq. (4) and the letter L is short for Love waves.

Once the cross-spectral densities $G_{R1T0}(r, r; \omega)$ and $G_{R1T0}(0, r; \omega)$ are calculated using field measurement records, it is quite straightforward to infer $c^L(\omega)$ by simple inversion of Eq. (4). The only input required is the two-component horizontal-motion records around a circle of radius r and at its center.

2.2 Method for Estimating the Power Share of Rayleigh Waves

Let $Z(t, r, \theta)$ be the vertical-motion seismogram of microtremors at radius r and azimuth θ, and let us define $Z_1(t, r)$ as a weighted average of $Z(t, r, \theta)$ over the azimuth θ:

$$Z_1(t,r) = \int_{-\pi}^{\pi} Z(t,r,\theta)\exp(-i\theta)d\theta . \quad (5)$$

We also define $R_0(t, r)$ as a non-weighted azimuthal average of $R(t, r, \theta)$:

$$R_0(t,r) = \int_{-\pi}^{\pi} R(t,r,\theta)d\theta . \quad (6)$$

Our formula for evaluating the share of Rayleigh waves in the total power of horizontal motion, which we denote by $\gamma^R(\omega)$, is

$$\gamma^R(\omega) = \frac{G_{Z0Z0}(0,0;\omega)\,G_{R0R0}(r,r;\omega)}{4G_{Z1Z1}(r,r;\omega)\,G_{R1R1}(0,0;\omega)} \quad (7)$$

(Tada et al., 2009, appendix C), where $G_{Z1Z1}(r, r; \omega)$ is the power-spectral density of $Z_1(t, r)$; $G_{R0R0}(r, r; \omega)$ is the power-spectral density of $R_0(t, r)$; $G_{R1R1}(0, 0; \omega)$ is the power-spectral density of $R_1(t, 0)$ (Eq. 2), which equals the sum of the power-spectral densities of the two horizontal components at the array center; and $G_{Z0Z0}(0, 0; \omega)$ is the power-spectral density of vertical motion at the center. Eq. (7) holds true under the assumption that (i) the field of microtremors is composed of Rayleigh and Love waves alone, and that (ii) the field of Rayleigh waves is dominated by a single mode (most typically the fundamental mode, but not necessarily). There is no theoretical requisite regarding the mode composition of Love waves. Because of assumption (i), the share of Love waves in the total power of horizontal motion is $1 - \gamma^R(\omega)$.

Once the four power-spectral densities appearing in Eq. (7) are calculated using field records, $\gamma^R(\omega)$ can be inferred by means of simple forward algebra. The only input required is the Z- and R-component records around a circle of radius r, plus three-component records at its center.

2.3 The BIDO Software Package

Our above-described new techniques of Love-wave properties analysis, namely the SPAC+L method (Eq. 4) and the γ^R estimation method (Eq. 7), are both part of the software package BIDO, which we are offering free on the user's demand (visit our BIDO Web site: http://staff.aist.go.jp/ikuo-chou/bidodl_en.html). BIDO, which we named after the Japanese word *bidō* for microtremors, is a bundle of analysis codes that implement the SPAC method plus a number of kindred techniques which we have developed by expanding it. When fed with appropriately formatted input seismograms, BIDO produces, in both numerical and graphical output, estimates of quantities including:

(i) Rayleigh-wave phase velocities (c^R) [SPAC method (Aki 1957); CCA method (Cho et al. 2006a); noise-compensated CCA, H0, H1, and V methods (Tada et al. 2007); SPAC+R, SPAC-R, and CCA-R methods (Tada et al. 2009, appendix B)],

(ii) Love-wave phase velocities (c^L) [SPAC+L, SPAC-L and CCA-L methods (Tada et al. 2009)],

(iii) Share of Rayleigh waves in the total power of horizontal motion (γ^R) (Tada et al. 2009, appendix C),

(iv) Horizontal-to-vertical amplitude ratios (ellipticities) of Rayleigh waves (Cho et al. 2006b, appendix E),

(v) Horizontal-to-vertical spectral ratios (HVSRs) of total motion, and

(vi) Noise-to-signal (NS) power ratios in vertical motion (Cho et al. 2006a).

When the input data lack records at the array center, the output lacks (iii) γ^R and (vi) NS ratios. When the input is composed of vertical-motion records alone, the output lacks (ii) c^L, (iii) γ^R, (iv) ellipticities, and (v) HVSRs. When, on the contrary, the input is composed of horizontal-motion records alone, the output lacks (iii) γ^R, (iv) ellipticities, (v) HVSRs, and (vi) NS ratios.

2.4 Error Factors

There are at least three categories of factors which can introduce errors into the estimates of c^L and γ^R that are derived by way of Eqs (4) and (7) using field records.

One is called directional aliasing. The time series $R_1(t, r)$, $R_0(t, r)$, $T_0(t, r)$, and $Z_1(t, r)$, or weighted and non-weighted azimuthal averages of seismograms around a circle, have to be inferred, in practice, by summing up seismograms at a finite number of stations. This introduces errors in the estimates of the spectral densities appearing in Eqs (4) and (7), because information on the directional characteristics of microtremors slips away partially. The effects of directional aliasing grow larger with increasing frequency (e.g. Cho et al. 2006b, Okada 2006, Tada et al. 2007, Cho et al. 2008).

Another factor is the presence of multiple modes in surface waves (Rayleigh and Love waves). Eq. (4) relies on the assumption that all Love waves are made up of a single mode, whereas Eq. (7) presupposes that all Rayleigh waves consist of a single mode. When these assumptions fail, so does the accuracy of the c^L and γ^R estimates. Like directional aliasing, the effects of multiple modes tend to grow larger in higher frequency ranges.

The third factor, the presence of incoherent noise, affects Eq. (7) but not Eq. (4). This is because the power-spectral densities, appearing in Eq. (7), get inflated by amounts that depend on the power of noise, whereas the cross-spectral densities, appearing in Eq. (4), are not affected (Cho et al. 2006b).

Quantitative evaluation of these error factors is beyond the scope of the present study. For the convenience of future investigations, however, we present relevant mathematical formulas in the Appendix (Sections A.1-A.5).

A fourth category of error factors, or stochastic uncertainties due to the finite length of available data, were theorized and quantitatively evaluated by ourselves with reference to the H0, H1, and CCA methods (Tada et al. 2007) and the SPAC method (Cho et al. 2008). Theorization of stochastic uncertainties in Eqs (4) and (7), however, remains yet to be done (see Section A.6 in the Appendix).

3. FIELD IMPLEMENTATION

3.1 Input Data and Analysis Output

We applied the BIDO software package to real microtremor data from the field with a view to evaluating the relative content of Rayleigh and Love waves in them. The input data are the same as those described in the work of Tada et al. (2009): six data sets from two measurement sites, one lying in a quiet residential area in the northern suburbs of Tokyo (KSKB: Kasukabe), and the other close to a street of heavy traffic near central Tokyo (KIBA: Kiba Park). At each site, circular arrays of six seismic sensors, with five of them distributed evenly around a circle and the sixth at its center, were deployed successively at three different array radii of r = 3, 12, and 36 m. The data sampling rate was 100 Hz and the duration was 30 min in all measurement sessions.

Figures 1 and 2 show, in the left columns, the share of Rayleigh waves in the total power of horizontal motion (γ^R) evaluated with Eq. (7), and in the right columns, the phase velocities of Love waves (c^L) inferred with the SPAC+L method (Eq. 4). The bold curves in the γ^R plots and the plus signs in the c^L plots indicate averages of estimates obtained from different portions of the data. Standard deviations are indicated by pairs of thin curves in the γ^R plots and by vertical error bars in the c^L plots. In both categories of plots, the horizontal axis denotes the frequency. Incidentally, estimates of γ^R based on Eq. (7) may exceed unity, although the true values of γ^R should lie between 0 and 1.

3.2 Estimates of Love-Wave Velocities

In the c^L plots (right columns of Figures 1 and 2), the bold and smooth curves, sloping left up, indicate phase velocities of fundamental-mode Love waves that were calculated theoretically from subsurface soil structure models (see Tada et al. 2009 for details). The gray shades highlight frequency intervals where agreement between the theoretical and inferred c^L is relatively good. These shades were drawn by visual inspection, and their locations are not necessarily based on objective criteria.

The pairs of thin and smooth curves, sloping right up, correspond to wavelengths (λ^L) of twice and ten times the array radius r, respectively. The area bordered on both sides by a pair of these curves ($2r < \lambda^L < 10r$) gives a rule-of-thumb measure of the interval in which one can most typically expect to obtain relatively accurate estimates of c^L, even though there are obvious exceptions (e.g. KSKB, r = 36 m; KIBA, r = 12 m).

3.3 Estimates of the Power Share of Rayleigh Waves

We have highlighted the frequency intervals of good agreement between the theoretical and inferred c^L not only in the c^L plots but also in the plots of γ^R (left columns of Figures 1 and 2). We focus our attention on the estimates of γ^R in those highlighted intervals, although we still need theoretical and empirical evidences to find out the frequency ranges in which the γ^R estimates are the most reliable.

In the cases of (i) KSKB, r = 12 m, (ii) KSKB, r = 36 m, and (iii) KIBA, r = 36 m, the γ^R estimates, derived from Eq. (7), take values of around 0.2 everywhere in the highlighted frequency ranges. This implies that about 80% of all power of horizontal-motion microtremors is made of Love-wave components, in contrast to only about 20% for the Rayleigh-wave components.

In the other cases, namely (iv) KSKB, r = 3 m, (v) KIBA, r = 3 m, and (vi) KIBA, r = 12 m, the γ^R estimates vary significantly within the highlighted frequency intervals. In these cases, the highlighted intervals lie at higher frequencies than in cases (i)-(iii), and therefore are expected to be more susceptible to potential effects of directional aliasing and of multiple modes (Section 2.4). The reliability of the γ^R estimates in cases (iv)-(vi) should therefore be taken with more caution.

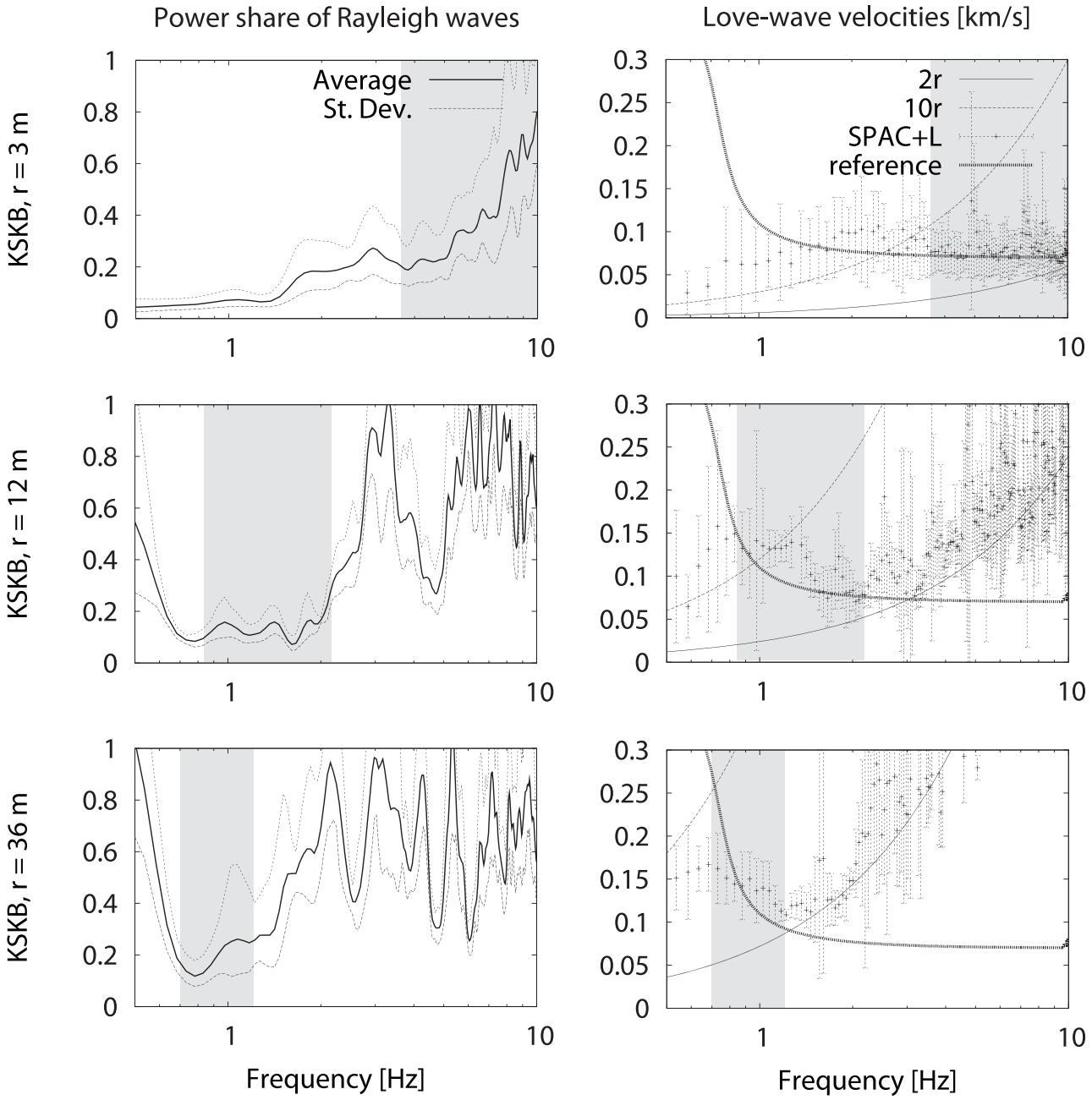

Figure 1 (Left) Share of Rayleigh waves in the total power of horizontal-motion microtremors (γ^R) at KSKB, evaluated using Eq. (7). The bold curves denote averages of estimates obtained from different portions of the data, whereas standard deviations are indicated by pairs of thin curves. The horizontal axis denotes the frequency.

From top to bottom, the plots show estimates using six-sensor, circular seismic arrays of radii r = 3, 12, and 36 m, respectively.

(Right) Phase velocities of Love waves (c^L) at KSKB, inferred with the SPAC+L method (Eq. 4). The plus signs denote averages of estimates obtained from different portions of the data, whereas standard deviations are indicated by vertical error bars. The horizontal axis denotes the frequency. The bold and smooth curves, sloping left up, indicate phase velocities of fundamental-mode Love waves that were derived theoretically from a subsurface soil structure model (Tada et al. 2009). The pairs of thin and smooth curves, sloping right up, correspond to wavelengths of twice and ten times the array radius r, respectively.

The shades highlight frequency intervals where agreement between the theoretical and inferred Love-wave phase velocities is relatively good.

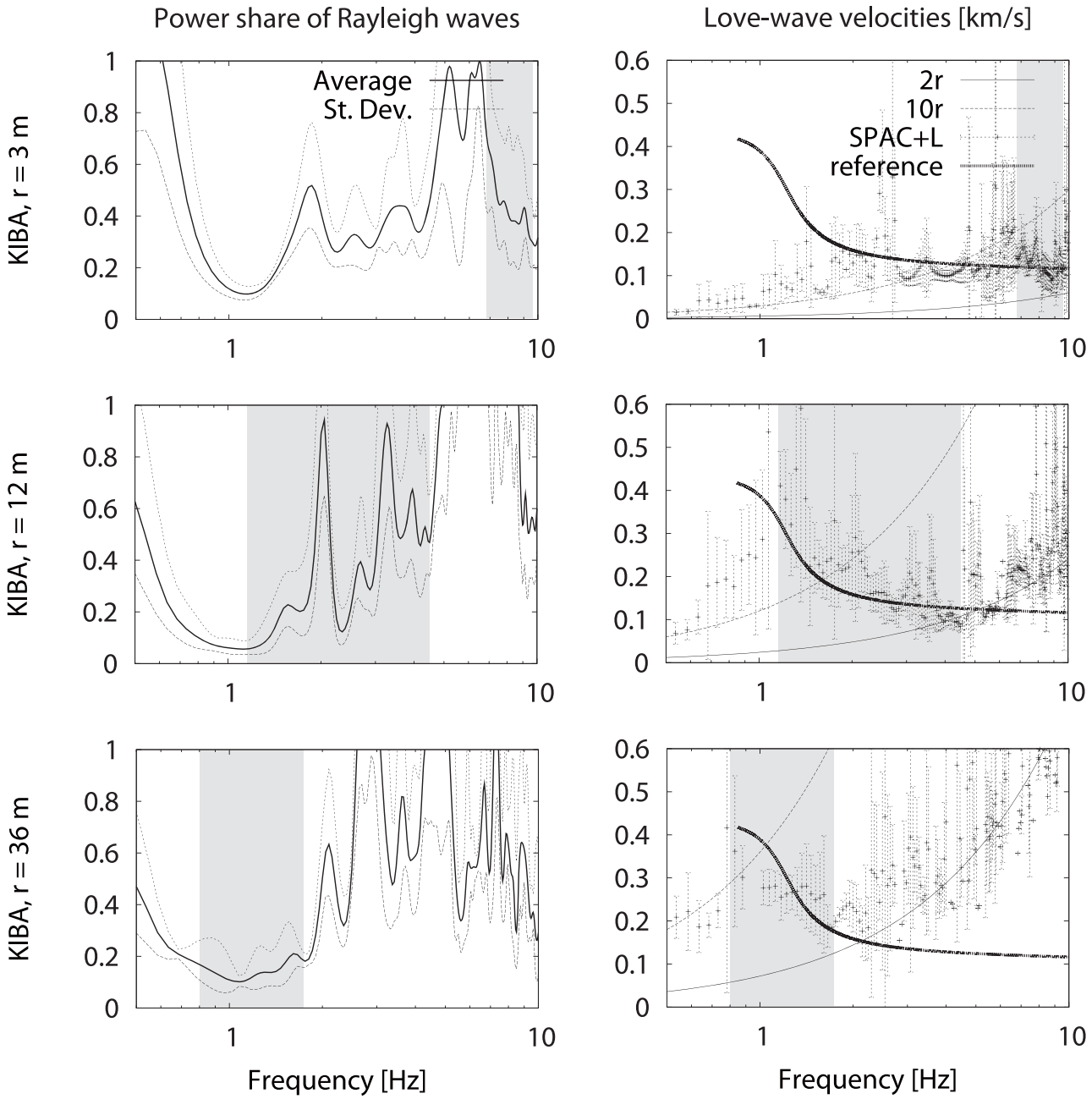

Figure 2 (Left) Share of Rayleigh waves in the total power of horizontal-motion microtremors (γ^R) at KIBA, evaluated using Eq. (7). (Right) Phase velocities of Love waves (c^L) at KIBA, inferred with the SPAC+L method (Eq. 4). From top to bottom, the plots show estimates using six-sensor, circular seismic arrays of radii r = 3, 12, and 36 m, respectively.

See caption to Figure 1 for the meaning of the curves, symbols and shades. The theoretical c^L dispersion curves (the bold and smooth curves that slope left up in the right column panels) are due to Tada et al. (2009).

A closer look reveals that γ^R estimates in the highlighted frequency bands stay around 0.2 everywhere if we limit our attention on low frequency ranges of less than 2 Hz (cases (i)-(iii) and part of case (vi)).

Previous studies that used the three-component SPAC method (Section 1) to evaluate γ^R in microtremors argued that the power of Rayleigh waves accounted for about half (Métaxian et al. 1997, Saccorotti et al. 2003) or less than half (Matsushima and Okada 1990, Arai and Tokimatsu 1998, Chouet et al. 1998, Yamamoto 2000, Köhler et al. 2007) of the total power of horizontal motion. Endrun et al. (2010) found γ^R to be variable, but consistently found it to be either at about half or below half. The results of our present study, implying the preponderance of Love waves, largely agree with the arguments of those earlier investigations.

4. CONCLUSION

We have applied new techniques of circular-array microtremor analysis to field data from two sites in the Tokyo conurbation. The results implied preponderance of Love waves over Rayleigh-wave components in horizontal-motion microtremors, at least in relatively low frequency ranges of less than 2 Hz. This finding is largely consistent with the arguments made by earlier studies, although further investigations are necessary before any conclusion can be drawn with certainty.

Ratios of power partition between Rayleigh and Love waves play an important part, e.g., in methods to interpret subsurface soil structures using horizontal-to-vertical spectral ratios (HVSRs) of microtremors. In practice, however, power partition ratio values have often been prescribed *a priori* (e.g. Arai and Tokimatsu 2004). Accumulation of reliable estimates for the power partition ratios should therefore be useful for enhancing the precision and utility of the microtremor HVSR exploration methods.

Acknowledgements:

The present work was partially supported by Grants-in-Aid for Scientific Research of the Japan Society for the Promotion of Science (JSPS) and of the Japanese Ministry of Education, Culture, Sports, Science, and Technology (MEXT).

References:

Aki, K. (1957), "Space and Time Spectra of Stationary Stochastic Waves, with Special Reference to Microtremors," *Bulletin of the Earthquake Research Institute, University of Tokyo*, **35**(3), 415-457.

Arai, H. and Tokimatsu, K. (1998), "Evaluation of Local Site Effects Based on Microtremor H/V Spectra," in *The Effects of Surface Geology on Seismic Motion*, Irikura, K., Kudo, K., Okada, H., and Sasatani, T. (editors), Balkema, Rotterdam, **2**, 673-680.

Arai, H. and Tokimatsu, K. (2004), "*S*-Wave Velocity Profiling by Inversion of Microtremor H/V Spectrum," *Bulletin of the Seismological Society of America*, **94**(1), 53-63.

Cho, I., Tada, T., and Shinozaki, Y. (2006a), "Centerless Circular Array Method: Inferring Phase Velocities of Rayleigh Waves in Broad Wavelength Ranges Using Microtremor Records," *Journal of Geophysical Research*, American Geophysical Union, **111**, B09315, doi:10.1029/2005JB004235.

Cho, I., Tada, T., and Shinozaki, Y. (2006b), "A Generic Formulation for Microtremor Exploration Methods Using Three-Component Records from a Circular Array," *Geophysical Journal International*, **165**(1), 236-258.

Cho, I., Tada, T., and Shinozaki, Y. (2008), "Assessing the Applicability of the Spatial Autocorrelation Method: A Theoretical Approach," *Journal of Geophysical Research*, American Geophysical Union, **113**, B06307, doi:10.1029/2007JB005245.

Chouet, B., De Luca, G., Milana, G., Dawson, P., Martini, M., and Scarpa, R. (1998), "Shallow Velocity Structure of Stromboli Volcano, Italy, Derived from Small-Aperture Array Measurements of Strombolian Tremor," *Bulletin of the Seismological Society of America*, **88**(3), 653-666.

Ekström, G., Abers, G. A., and Webb, S. C. (2009), "Determination of Surface-Wave Phase Velocities across USArray from Noise and Aki's Spectral Formulation," *Geophysical Research Letters*, American Geophysical Union, **36**, L18301, doi:10.1029/2009GL039131.

Endrun, B., Ohrnberger, M., and Savvaidis, A. (2010), "On the Repeatability and Consistency of Three-Component Ambient Vibration Array Measurements," *Bulletin of Earthquake Engineering*, in press, doi:10.1007/s10518-009-9159-9.

Ferrazzini, V., Aki, K., and Chouet, B. (1991), "Characteristics of Seismic Waves Composing Hawaiian Volcanic Tremor and Gas-Piston Events Observed by a Near-Source Array," *Journal of Geophysical Research*, American Geophysical Union, **96**(B4), 6199-6209.

Köhler, A., Ohrnberger, M., Scherbaum, F., Wathelet, M., and Cornou, C. (2007), "Assessing the Reliability of the Modified Three-Component Spatial Autocorrelation Technique," *Geophysical Journal International*, **168**(2), 779-796.

Matsushima, T. and Okada, H. (1990), "An Exploration Method Using Microtremors (2)—An Experiment to Identify Love Waves in Long-Period Microtremors" (in Japanese with English abstract), *Proceedings of the 82nd SEGJ Conference*, Society of Exploration Geophysicists of Japan, 5-8.

Métaxian, J.-P., Lesage, P., and Dorel, J. (1997), "Permanent Tremor of Masaya Volcano, Nicaragua: Wave Field Analysis and Source Location," *Journal of Geophysical Research*, American Geophysical Union, **102**(B10), 22,529-22,545.

Okada, H. (2006), "Theory of Efficient Array Observations of Microtremors with Special Reference to the SPAC Method," *Exploration Geophysics*, Australian Society of Exploration Geophysicists, **37**(1); *Butsuri-Tansa*, Society of Exploration Geophysicists of Japan, **59**(1); *Mulli-Tamsa*, Korean Society of Exploration Geophysicists, **9**(1), 73-85.

Okada, H. and Matsushima, T. (1989), "An Exploration Method Using Microtremors (1)—A Theory to Identify Love Waves in Microtremors" (in Japanese with English abstract), *Proceedings of the 81st SEGJ Conference*, Society of Exploration Geophysicists of Japan, 15-18.

Picozzi, M., Strollo, A., Parolai, S., Durukal, E., Özel, O., Karabulut, S., Zschau, J., and Erdik, M. (2009), "Site Characterization by Seismic Noise in Istanbul, Turkey," *Soil Dynamics and Earthquake Engineering*, **29**(3), 469-482.

Prieto, G. A., Lawrence, J. F., and Beroza, G. C. (2009), "Anelastic Earth Structure from the Coherency of the Ambient Seismic Field," *Journal of Geophysical Research*, American Geophysical Union, **114**, B07303, doi:10.1029/2008JB006067.

Saccorotti, G., Chouet, B., and Dawson, P. (2003), "Shallow-Velocity Models at the Kilauea Volcano, Hawaii, Determined from Array Analyses of Tremor Wavefields," *Geophysical Journal International*, **152**(3), 633-648.

Stephenson, W. J., Hartzell, S., Frankel, A. D., Asten, M., Carver, D. L., and Kim, W. Y. (2009), "Site Characterization for Urban Seismic Hazards in Lower Manhattan, New York City, from Microtremor Array Analysis," *Geophysical Research Letters*, American Geophysical Union, **36**, L03301,

doi:10.1029/2008GL036444.
Tada, T., Cho, I., and Shinozaki, Y. (2007), "Beyond the SPAC Method: Exploiting the Wealth of Circular-Array Methods for Microtremor Exploration," *Bulletin of the Seismological Society of America*, **97**(6), 2080-2095.
Tada, T., Cho, I., and Shinozaki, Y. (2009), "New Circular-Array Microtremor Techniques to Infer Love-Wave Phase Velocities," *Bulletin of the Seismological Society of America*, **99**(5), 2912-2926.
Yamamoto, H. (2000), "An Experiment for Estimating Phase Velocities of Love Waves from Three-Component Microtremor Array Observations" (in Japanese with English abstract), *Butsuri-Tansa*, Society of Exploration Geophysicists of Japan, **53**(2), 153-166.

APPENDIX. EFFECTS OF DIRECTIONAL ALIASING, MULTIPLE MODES OF SURFACE WAVES, AND INCOHERENT NOISE

In this appendix we present mathematical formulas that describe the effects of the three error factors mentioned in Section 2.4—directional aliasing, multiple modes of surface waves, and incoherent noise—on the estimates of the quantities given by Eqs (4) and (7). Numerical evaluation of these error factors, however, is beyond the scope of the present paper and we leave that for future investigations.

A.1 Basic Formula of Directional Aliasing

Let us denote, by the letter X, either one of the three letters R, T, and Z, which stand for the radial-, transverse-, and vertical-component seismograms of microtremors, respectively. Let us also denote, by

$$X_m(t,r) = \int_{-\pi}^{\pi} X(t,r,\theta)\exp(-im\theta)d\theta\,, \qquad \text{(A.1)}$$

the mth-order coefficient in the Fourier series expansion of $X(t, r, \theta)$ with respect to the azimuth θ. Under the assumption that (i) a finite number of N seismic sensors are distributed evenly around a circle of radius r, with one of them lying in the direction of zero azimuth, the estimate for $X_m(t, r)$, obtained by taking a weighted sum of seismograms at the N stations, is related to the true values of $X_m(t, r)$ by

$$\hat{X}_m(t,r) = \sum_{j=-\infty}^{\infty} X_{m+jN}(t,r) \qquad \text{(A.2)}$$

(e.g. Cho et al. 2006b).

There is no directional aliasing when $r = 0$.

A.2 Notation for the Modes of Surface Waves

We use the letter q to denote the qth mode of surface waves (Rayleigh or Love waves), and N^R and N^L to denote the total number of modes for the Rayleigh and Love waves, respectively.

A.3 Cross- and Power-Spectral Densities of Incoherent Noise

Let $G_{XmYn}(r_1, r_2; \omega)$ denote the cross-spectral density between two time series $X_m(t, r_1)$ and $Y_n(t, r_2)$. When the latter two represent Fourier coefficients of an identical order ($m = n$) for an identical component ($X = Y$) of seismograms around an identical circle ($r_1 = r_2 = r$), $G_{XmYn}(r_1, r_2; \omega) = G_{XmXm}(r, r; \omega)$ represents the power-spectral density of the time series $X_m(t, r)$.

Suppose that (ii) seismograms include noise that is uncorrelated with the microtremor signals (i.e. propagating Rayleigh- and Love-wave components). In this case, the estimate (which we indicate by a superscript hat) of the cross- or power-spectral density $G_{XmYn}(r_1, r_2; \omega)$, obtained using the noise-inclusive seismograms, equals the sum of a spectral density estimate relevant to the signals (which we indicate by a superscript s) and a spectral density estimate relevant to the noise (which we denote by a superscript n):

$$\hat{G}_{XmYn}(r_1,r_2;\omega) = \hat{G}^{s}_{XmYn}(r_1,r_2;\omega) + \hat{G}^{n}_{XmYn}(r_1,r_2;\omega)\,. \qquad \text{(A.3)}$$

The signal term includes the effects of both directional aliasing and multiple modes.

If (iii) the noise is incoherent (uncorrelated) from one sensor to another, the noise term in Eq. (A.3) is non-zero when and only when the two radii, r_1 and r_2, coincide.

If (iv) the noise is incoherent from one component to another in the records of an identical sensor, the noise term in Eq. (A.3) is non-zero when and only when the combination of the two component indicators, (X, Y), is either (Z, Z), (R, R), (T, T), (R, T), or (T, R). The noise term does not necessarily vanish for (R, T) and (T, R), because both the R and T records contain contributions from the east-west and north-south component seismograms.

Let us further assume that (v) the noise has identical intensities for all sensors, that (vi) the noise has identical intensities for the two components of horizontal motion at an identical station, and that (i) N seismic stations are distributed at equal distances around a circle of radius r. Cho et al. (2006b) demonstrated that, for $r \neq 0$,

$$\hat{G}^{n}_{ZmZn}(r,r;\omega) = 4\pi^2\delta_{mn}f_Z(\omega)/N \qquad \text{(A.4)}$$

$$\hat{G}^{n}_{RmRn}(r,r;\omega) = \hat{G}^{n}_{TmTn}(r,r;\omega) = 2\pi^2\delta_{mn}f_H(\omega)/N \qquad \text{(A.5)}$$

$$\hat{G}^{n}_{RmTn}(r,r;\omega) = \hat{G}^{n}_{TmRn}(r,r;\omega) = 0\,, \qquad \text{(A.6)}$$

where δ_{mn} denotes the Kronecker delta, $f_Z(\omega)$ is the power of noise in vertical motion, and $f_H(\omega)$ is the total power of noise in the two components of horizontal motion. The power of noise in either the east-west or the north-south component is given by (1/2) $f_H(\omega)$. Eqs (A.4)-(A.6) indicate that the noise term in Eq. (A.3) is non-zero when and only when the two component indicators, X and Y, are identical (the combinations (R, T) and (T, R) are no longer included), and the two order numbers, m and n, are also identical.

For the case of $r_1 = r_2 = 0$, Cho et al. (2006b)

demonstrated that

$$\hat{G}^{n}_{Z0Z0}(0,0;\omega) = 4\pi^2 f_Z(\omega) \tag{A.7}$$

$$\hat{G}^{n}_{R1R1}(0,0;\omega) = \hat{G}^{n}_{T1T1}(0,0;\omega) = \pi^2 f_H(\omega) \tag{A.8}$$

$$\hat{G}^{n}_{R1T1}(0,0;\omega) = -i\pi^2 f_H(\omega)\,. \tag{A.9}$$

A.4 SPAC+L Method

Let us denote, by $\rho_{\mathrm{SPAC+L}}$, the spectral ratio that appears on the left-hand side of Eq. (4):

$$\rho_{\mathrm{SPAC+L}} = \frac{G_{R1T0}(r,r;\omega)}{G_{R1T0}(0,r;\omega)}\,. \tag{A.10}$$

Both the denominator, $G_{R1T0}(0, r; \omega)$, and the numerator, $G_{R1T0}(r, r; \omega)$, are free from the effects of incoherent noise under the assumptions described in Section A.3:

$$\hat{G}^{n}_{R1T0}(0,r;\omega) = \hat{G}^{n}_{R1T0}(r,r;\omega) = 0\,. \tag{A.11}$$

The denominator is the cross-spectral density (which we denote CSD in equations that follow) between the estimates of $R_1(t, 0)$ and $T_0(t, r)$. Its estimate, to be obtained by records of N sensors around the circle, is

$$\begin{aligned}
\hat{G}_{R1T0}(0,r;\omega) &= \hat{G}^{s}_{R1T0}(0,r;\omega) = \mathrm{CSD}[\hat{R}_1(t,0), \hat{T}_0(t,r)] \\
&= \mathrm{CSD}\left[R_1(t,0), \sum_{j=-\infty}^{\infty} T_{jN}(t,r) \right] \\
&= \sum_{j=-\infty}^{\infty} \mathrm{CSD}[R_1(t,0), T_{jN}(t,r)] \\
&= \sum_{j=-\infty}^{\infty} G_{R1T(jN)}(0,r;\omega)\,.
\end{aligned} \tag{A.12}$$

All terms other than $j = 0$ represent the effects of directional aliasing.

A general mathematical expression for $G_{RmTn}(r_1, r_2; \omega)$, in the presence of multiple modes of surface waves, is given in the work of Tada et al. (2009, eq. 18). Substituting that expression into Eq. (A.12), one obtains

$$\begin{aligned}
\hat{G}_{R1T0}(0,r;\omega) = -\pi^2 \sum_{j=-\infty}^{\infty} &\exp(ijN\pi/2) \\
\times \Bigg[&\sum_{q=1}^{N^R} (J_{jN-1} + J_{jN+1})(rk_q^R(\omega))\, f^R_{q/-jN+1}(\omega) \\
&+ \sum_{q=1}^{N^L} (J_{jN-1} - J_{jN+1})(rk_q^L(\omega))\, f^L_{q/-jN+1}(\omega) \Bigg].
\end{aligned} \tag{A.13}$$

In Eq. (A.13), $k_q^R(\omega) = \omega / c_q^R(\omega)$ represents the wavenumber of the qth-mode Rayleigh waves, whereas $f_{q/m}^R(\omega)$ denotes the mth-order component in the Fourier series expansion of the intensity-versus-arrival-azimuth profile of the qth-mode Rayleigh waves in horizontal motion—the component that undulates sinusoidally over m cycles during one rotation. The symbols $k_q^L(\omega)$ and $f_{q/m}^L(\omega)$ denote the Love-wave counterparts of $k_q^R(\omega)$ and $f_{q/m}^R(\omega)$.

For the sake of simplicity, we introduce two additional assumptions here: (vii) $N \geq 3$, and (viii) $f_{q/m}^R(\omega) = f_{q/m}^L(\omega) = 0$ for all $m \geq 2$ and $m \leq -2$. The latter assumption means that the intensity-versus-arrival-azimuth profile of the surface waves is made up only of a homogeneous (or isotropic) component ($m = 0$) plus dipolar components ($m = \pm 1$). These assumptions eliminate all terms with $j \neq 0$ in Eq. (A.13):

$$\hat{G}_{R1T0}(0,r;\omega) = 2\pi^2 \sum_{q=1}^{N^L} f^L_{q/1}(\omega)\, J_1(rk_q^L(\omega))\,. \tag{A.14}$$

Likewise, the estimate for the numerator is

$$\begin{aligned}
\hat{G}_{R1T0}(r,r;\omega) &= \hat{G}^{s}_{R1T0}(r,r;\omega) = \mathrm{CSD}[\hat{R}_1(t,r), \hat{T}_0(t,r)] \\
&= \mathrm{CSD}\left[\sum_{j=-\infty}^{\infty} R_{1+jN}(t,r), \sum_{l=-\infty}^{\infty} T_{lN}(t,r) \right] \\
&= \sum_{j,l=-\infty}^{\infty} \mathrm{CSD}[R_{1+jN}(t,r), T_{lN}(t,r)] \\
&= \sum_{j,l=-\infty}^{\infty} G_{R(1+jN)T(lN)}(r,r;\omega)\,.
\end{aligned} \tag{A.15}$$

All terms other than $j = l = 0$ represent the effects of directional aliasing. Substituting eq. (18) of Tada et al. (2009) into Eq. (A.15), one obtains

$$\begin{aligned}
\hat{G}_{R1T0}(r,r;\omega) = -\pi^2 \sum_{j,l=-\infty}^{\infty} &\exp\left[i(l-j)N\pi/2\right] \\
\times \Bigg[&\sum_{q=1}^{N^R} (J_{jN} - J_{jN+2})(rk_q^R(\omega)) \\
&\times (J_{lN-1} + J_{lN+1})(rk_q^R(\omega))\, f^R_{q/(j-l)N+1}(\omega) \\
&+ \sum_{q=1}^{N^L} (J_{jN} + J_{jN+2})(rk_q^L(\omega)) \\
&\times (J_{lN-1} - J_{lN+1})(rk_q^L(\omega))\, f^L_{q/(j-l)N+1}(\omega) \Bigg].
\end{aligned} \tag{A.16}$$

Assumptions (vii) and (viii) eliminate all terms other than $j = l$ in Eq. (A.16):

$$\hat{G}_{R1T0}(r,r;\omega) = -\pi^2 \sum_{q=1}^{N^R} f_{q/1}^R(\omega) \sum_{j=-\infty}^{\infty} (J_{jN} - J_{jN+2})(rk_q^R(\omega)) \times (J_{jN-1} + J_{jN+1})(rk_q^R(\omega)) - \pi^2 \sum_{q=1}^{N^L} f_{q/1}^L(\omega) \sum_{j=-\infty}^{\infty} (J_{jN} + J_{jN+2})(rk_q^L(\omega)) \times (J_{jN-1} - J_{jN+1})(rk_q^L(\omega)). \quad (A.17)$$

Finally, the estimate for the spectral ratio $\rho_{\mathrm{SPAC+L}}$, to be obtained by using the cross-spectral density estimates (A.14) and (A.17) in Eq. (A.10), is given by

$$\hat{\rho}_{\mathrm{SPAC+L}} = \frac{\hat{G}_{R1T0}(r,r;\omega)}{\hat{G}_{R1T0}(0,r;\omega)} = -\left[\sum_{q=1}^{N^R} f_{q/1}^R(\omega) \sum_{j=-\infty}^{\infty} (J_{jN} - J_{jN+2})(rk_q^R(\omega)) \times (J_{jN-1} + J_{jN+1})(rk_q^R(\omega)) + \sum_{q=1}^{N^L} f_{q/1}^L(\omega) \sum_{j=-\infty}^{\infty} (J_{jN} + J_{jN+2})(rk_q^L(\omega)) \times (J_{jN-1} - J_{jN+1})(rk_q^L(\omega)) \right] \Bigg/ \left[2\sum_{q=1}^{N^L} f_{q/1}^L(\omega) J_1(rk_q^L(\omega)) \right]. \quad (A.18)$$

In Eq. (A.18), all terms other than $j = 0$, involving Bessel functions of the third or higher orders (recall our assumption (vii) that $N \geq 3$), represent the effects of directional aliasing. Summations over q represent the effects of multiple modes. Both effects remain insignificant in low frequency ranges ($rk^R(\omega) = r\omega/c^R(\omega)$ and $rk^L(\omega) = r\omega/c^L(\omega)$ tend to zero when $\omega \rightarrow 0$). The point where they cease to be negligible defines the upper limit on the valid frequency range of the SPAC+L method.

To the extent that our assumptions stated in Section A.3 are valid, the effects of incoherent noise do not enter Eq. (A.18). It therefore remains beyond one's power, as long as one relies on the theoretical framework presented here, to evaluate how noise affects or limits the validity of the SPAC+L method.

A.5 Power Partition Ratio Estimation Method

The four power-spectral densities, which enter Eq. (7), are all subject to the effects of incoherent noise, and their magnitudes are given by Eqs (A.4), (A.5), (A.7), and (A.8). Let us introduce new symbols, $\varepsilon_Z(\omega)$ and $\varepsilon_H(\omega)$, for the noise-to-signal (NS) power ratios of the vertical and horizontal motions, respectively:

$$\varepsilon_Z(\omega) = \frac{f_Z(\omega)}{\sum_{q=1}^{N^R} |h_q(\omega)|^2 \, f_{q/0}^R(\omega)} \quad (A.19)$$

$$\varepsilon_H(\omega) = \frac{f_H(\omega)}{\sum_{q=1}^{N^R} f_{q/0}^R(\omega) + \sum_{q=1}^{N^L} f_{q/0}^L(\omega)}. \quad (A.20)$$

In Eqs (A.19)-(A.20), the quantities $f_{q/0}{}^R(\omega)$ and $f_{q/0}{}^L(\omega)$ correspond to the horizontal-motion intensity, in the most usual definition of the word, of the qth mode of Rayleigh and Love waves, respectively, whereas $|h_q(\omega)|$ denotes the vertical-to-horizontal amplitude ratio of the qth-mode Rayleigh waves. Using these symbols, the noise terms (see Eq. A.3) in the power-spectral density estimates may be rewritten as

$$\hat{G}_{Z0Z0}^n(0,0;\omega) = 4\pi^2 \varepsilon_Z(\omega) \sum_{q=1}^{N^R} |h_q(\omega)|^2 \, f_{q/0}^R(\omega) \quad (A.21)$$

$$\hat{G}_{Z1Z1}^n(r,r;\omega) = 4\pi^2 \frac{\varepsilon_Z(\omega)}{N} \sum_{q=1}^{N^R} |h_q(\omega)|^2 \, f_{q/0}^R(\omega) \quad (A.22)$$

$$\hat{G}_{R1R1}^n(0,0;\omega) = \pi^2 \varepsilon_H(\omega) \left[\sum_{q=1}^{N^R} f_{q/0}^R(\omega) + \sum_{q=1}^{N^L} f_{q/0}^L(\omega) \right] \quad (A.23)$$

$$\hat{G}_{R0R0}^n(r,r;\omega) = 2\pi^2 \frac{\varepsilon_H(\omega)}{N} \left[\sum_{q=1}^{N^R} f_{q/0}^R(\omega) + \sum_{q=1}^{N^L} f_{q/0}^L(\omega) \right]. \quad (A.24)$$

In the meantime, general mathematical expressions for $G_{ZmZn}(r_1, r_2; \omega)$ and $G_{RmRn}(r_1, r_2; \omega)$, in the presence of multiple modes, are presented in the works of Cho et al. (2006b, eqs 58-59) and Tada et al. (2009, eqs A7-A8). Using those formulas, and applying assumptions (vii) and (viii) that were described in Section A.4, we obtain the following expressions for the signal terms (see Eq. A.3) in the power-spectral density estimates:

$$\hat{G}_{Z0Z0}^s(0,0;\omega) = G_{Z0Z0}(0,0;\omega) = 4\pi^2 \sum_{q=1}^{N^R} |h_q(\omega)|^2 \, f_{q/0}^R(\omega) \quad (A.25)$$

$$\hat{G}_{Z1Z1}^s(r,r;\omega) = \sum_{j,l=-\infty}^{\infty} G_{Z(1+jN)Z(1+lN)}(r,r;\omega) = 4\pi^2 \sum_{q=1}^{N^R} |h_q(\omega)|^2 \, f_{q/0}^R(\omega) \sum_{j=-\infty}^{\infty} J_{jN+1}^2(rk_q^R(\omega)) \quad (A.26)$$

$$\hat{G}_{R1R1}^s(0,0;\omega) = G_{R1R1}(0,0;\omega) = \pi^2 \left[\sum_{q=1}^{N^R} f_{q/0}^R(\omega) + \sum_{q=1}^{N^L} f_{q/0}^L(\omega) \right] \quad (A.27)$$

$$\hat{G}^{s}_{R0R0}(r,r;\omega) = \sum_{j,l=-\infty}^{\infty} G_{R(jN)R(lN)}(r,r;\omega)$$
$$= \pi^2 \sum_{q=1}^{N^R} f^R_{q/0}(\omega) \sum_{j=-\infty}^{\infty} (J_{jN-1} - J_{jN+1})^2 (rk^R_q(\omega))$$
$$+ \pi^2 \sum_{q=1}^{N^L} f^L_{q/0}(\omega) \sum_{j=-\infty}^{\infty} (J_{jN-1} + J_{jN+1})^2 (rk^L_q(\omega)). \quad \text{(A.28)}$$

Directional aliasing terms ($j \neq 0$) appear in the estimates of $G_{Z1Z1}(r, r; \omega)$ and $G_{R0R0}(r, r; \omega)$, which use records around the circle (Eqs A.26 and A.28), but do not do so in the estimates of $G_{Z0Z0}(0, 0; \omega)$ and $G_{R1R1}(0, 0; \omega)$, which use records at the center alone (Eqs A.25 and A.27).

Adding up the signal terms and noise terms, we get

$$\hat{G}_{Z0Z0}(0,0;\omega) = \hat{G}^{s}_{Z0Z0}(0,0;\omega) + \hat{G}^{n}_{Z0Z0}(0,0;\omega)$$
$$= 4\pi^2 (1 + \varepsilon_Z(\omega)) \sum_{q=1}^{N^R} |h_q(\omega)|^2 f^R_{q/0}(\omega) \quad \text{(A.29)}$$

$$\hat{G}_{Z1Z1}(r,r;\omega) = \hat{G}^{s}_{Z1Z1}(r,r;\omega) + \hat{G}^{n}_{Z1Z1}(r,r;\omega)$$
$$= 4\pi^2 \sum_{q=1}^{N^R} |h_q(\omega)|^2 f^R_{q/0}(\omega) \left[\sum_{j=-\infty}^{\infty} J^2_{jN+1}(rk^R_q(\omega)) + \frac{\varepsilon_Z(\omega)}{N} \right] \quad \text{(A.30)}$$

$$\hat{G}_{R1R1}(0,0;\omega) = \hat{G}^{s}_{R1R1}(0,0;\omega) + \hat{G}^{n}_{R1R1}(0,0;\omega)$$
$$= \pi^2 (1 + \varepsilon_H(\omega)) \left[\sum_{q=1}^{N^R} f^R_{q/0}(\omega) + \sum_{q=1}^{N^L} f^L_{q/0}(\omega) \right] \quad \text{(A.31)}$$

$$\hat{G}_{R0R0}(r,r;\omega) = \hat{G}^{s}_{R0R0}(r,r;\omega) + \hat{G}^{n}_{R0R0}(r,r;\omega)$$
$$= \pi^2 \sum_{q=1}^{N^R} f^R_{q/0}(\omega) \left[\sum_{j=-\infty}^{\infty} (J_{jN-1} - J_{jN+1})^2 (rk^R_q(\omega)) + \frac{2\varepsilon_H(\omega)}{N} \right]$$
$$+ \pi^2 \sum_{q=1}^{N^L} f^L_{q/0}(\omega) \left[\sum_{j=-\infty}^{\infty} (J_{jN-1} + J_{jN+1})^2 (rk^L_q(\omega)) + \frac{2\varepsilon_H(\omega)}{N} \right]. \quad \text{(A.32)}$$

Finally, the estimate for the power share of Rayleigh waves, $\gamma^R(\omega)$, to be obtained by using the power-spectral density estimates (A.29)-(A.32) in Eq. (A.7), is given by

$$\hat{\gamma}^R(\omega) = \frac{\hat{G}_{Z0Z0}(0,0;\omega)\, \hat{G}_{R0R0}(r,r;\omega)}{4\hat{G}_{Z1Z1}(r,r;\omega)\, \hat{G}_{R1R1}(0,0;\omega)}$$
$$= \frac{1 + \varepsilon_Z(\omega)}{1 + \varepsilon_H(\omega)}$$
$$\times \left[\frac{\sum_{q=1}^{N^R} f^R_{q/0}(\omega) \sum_{j=-\infty}^{\infty} (J_{jN-1} - J_{jN+1})^2 (rk^R_q(\omega))}{4\left(\sum_{q=1}^{N^R} f^R_{q/0}(\omega) + \sum_{q=1}^{N^L} f^L_{q/0}(\omega) \right)} + \frac{\varepsilon_H(\omega)}{2N} \right]$$
$$+ \frac{\sum_{q=1}^{N^L} f^L_{q/0}(\omega) \sum_{j=-\infty}^{\infty} (J_{jN-1} + J_{jN+1})^2 (rk^L_q(\omega))}{4\left(\sum_{q=1}^{N^R} f^R_{q/0}(\omega) + \sum_{q=1}^{N^L} f^L_{q/0}(\omega) \right)} + \frac{\varepsilon_H(\omega)}{2N} \Bigg]$$
$$\Bigg/ \left[\frac{\sum_{q=1}^{N^R} |h_q(\omega)|^2 f^R_{q/0}(\omega) \sum_{j=-\infty}^{\infty} J^2_{jN+1}(rk^R_q(\omega))}{\sum_{q=1}^{N^R} |h_q(\omega)|^2 f^R_{q/0}(\omega)} + \frac{\varepsilon_Z(\omega)}{N} \right]. \quad \text{(A.33)}$$

In Eq. (A.33), all terms other than $j = 0$, involving Bessel functions of the second or higher orders, represent the effects of directional aliasing. Summations over q represent the effects of multiple modes. The effects of incoherent noise enters Eq. (A.33) by way of the NS ratios, $\varepsilon_Z(\omega)$ and $\varepsilon_H(\omega)$.

The effects of directional aliasing and multiple modes remain insignificant in low frequency ranges, and the point where they cease to be negligible defines the upper bound on the valid frequency range of the γ^R estimation method.

The effects of incoherent noise, on the contrary, are the most significant in low frequency ranges. The point where $J_1(rk^R(\omega))$ of the fundamental-mode Rayleigh waves becomes so small that $\varepsilon_Z(\omega)/N$ and $\varepsilon_H(\omega)/N$ are no longer negligible in comparison to $J_1^2(rk^R(\omega))$ defines the lower bound on the valid frequency range of the γ^R estimation method. Using the asymptotic expression for the Bessel function $J_1(\cdot)$ near a zero argument, this lower bound may be redefined as the frequency ω that satisfies

$$\frac{(rk^R(\omega))^2}{4} \approx \max\left(\frac{\varepsilon_Z(\omega)}{N}, \frac{\varepsilon_H(\omega)}{N} \right). \quad \text{(A.34)}$$

A.6 Stochastic Uncertainties

The quantities given by Eqs (4) and (7) should be subject to a fourth category of error factors, namely stochastic uncertainties arising from the finite length of available data (Section 2.4).

Tada et al. (2007) presented theoretical expressions for the magnitude of stochastic uncertainties with respect to a number of spectral ratios used in circular-array microtremor techniques. Their theoretical framework, however, works only for ratios of two power-spectral densities. Using a different approach, Cho et al. (2008) derived a mathematical expression for the magnitude of stochastic uncertainties accompanying the SPAC coefficient, a quantity playing a central role in the SPAC method. The SPAC coefficient has the form of a cross-spectral density divided by a power-spectral density.

Theorization remains yet to be done, however, for a ratio of two cross-spectral ratios, like Eq. (4), and for a ratio involving four power-spectral ratios, like Eq. (7).